THE UNIVERSITY OF ALBERTA

# ELECTRON BEAM MEASUREMENTS OF ACCOMMODATION COEFFICIENTS

by

GLEN STEPHEN SMYRL, B.Sc. (ALBERTA)

A THESIS

SUBMITTED TO THE FACULTY OF

GRADUATE STUDIES IN PARTIAL

FULFILMENT OF THE REQUIREMENTS FOR

THE DEGREE OF MASTER OF SCIENCE

DEPARTMENT OF MECHANICAL ENGINEERING

EDMONTON, ALBERTA

MAY , 1968

UNIVERSITY OF ALBERTA

FACULTY OF GRADUATE STUDIES

The undersigned certify that they have read, and recommend to the Faculty of Graduate Studies a thesis entitled, "ELECTRON BEAM MEASUREMENTS OF ACCOMMODATION COEFFICIENTS"submitted by GLEN STEPHEN SMYRL in partial fulfilment of the requirements for the degree of Master of Science.

# ABSTRACT

In this thesis an apparatus is developed to experimentally determine energy and normal momentum accommodation coefficients using an electron beam excited fluorescence density probe. These measurements required that the electron beam technique be extended to a lower density range than has previously been investigated.

A primary consideration in the design was the maintenance of a clean test surface for accommodation measurements. This was accomplished by the careful construction of the experimental apparatus and control of the cleanliness of the test gas being admitted to the system.

Accommodation measurements are shown to be practical with experimental scatter of less than 4.5 per cent.

## ACKNOWLEDGEMENTS

The author wishes to extend his appreciation to DR. D.J. MARSDEN for his guidance and supervision of this thesis and to the National Research Council for financial support.

Thanks are also extended to the members of the Mechanical Engineering Shop, who manufactured a large part of the experimental apparatus and to Miss Lynne Fiveland for her patience in typing the thesis.

# TABLE OF CONTENTS

## List of Symbols

| | | |
|---|---|---|
| $A$ | | area |
| $A_{mn}$ | | Einstein's spontaneous emission probability |
| $\underline{b}$ | | unit normal vector |
| $c$ | | molecular speed |
| $c_j$ | | $j^{th}$ component of molecular velocity |
| $c_m$ | = | $\sqrt{2RT}$ = most probable speed |
| $d$ | | distance from point P to plane of orifice |
| $D$ | | distance from point P to plane of optical lens |
| $E$ | | energy |
| $\tilde{e}$ | | energy per molecule crossing dA in time dt |
| $f$ | | velocity distribution function |
| $G$ | | solid angle/$4\pi$ |
| $G$ | | photomultiplier gain |
| $h$ | | Planck's constant |
| $i$ | | electron beam current |
| $I$ | | photomultiplier current |
| $k$ | | Boltzmann's constant |
| $K$ | | sensitivity of electron beam calibration |
| $m$ | | mass of a molecule |
| $M$ | | molecular weight |
| $n(x,t)$ | | molecular number density |
| $n_a$ | | contribution to number density at point P from molecules coming through orifice |

| | |
|---|---|
| $n_b$ | number density at point P due to background molecules |
| N | number of molecules crossing dA in time dt |
| P | normal momentum flux across dA in time dt |
| P | pressure |
| Q | mutual collision cross section for excitation |
| $r_o$ | radius of orifice |
| R | gas constant |
| $\Delta s$ | length of electron beam focused on photomultiplier |
| T | temperature |
| T | light transmission efficiency |
| t | time |
| u | macroscopic velocity component |
| $\underline{x}$ | position vector |
| $\alpha$ | energy accommodation coefficient |
| $\gamma$ | efficiency of electron beam measurement |
| $\sigma$ | collision cross section for nn' molecules |
| $\sigma'$ | normal momentum accommodation coefficient |
| $\underline{\xi}$ | molecular velocity vector |
| $\Phi$ | fluorescent light yield |
| $d\omega$ | solid angle |

Other symbols not defined here are defined when used.

# CHAPTER I

## 1. Introduction

During the last half century, much research has been done in an attempt to investigate the mechanisms of interaction between a rarefied gas and a solid surface. This research has been necessitated by the rapid advances made in high-altitude flight and in the fields of surface chemistry and physics.

When the mean free path of a gas is large as compared to a characteristic surface dimension, the energy of molecules reflected from a surface does not, in general, correspond to that which is characteristic of the surface temperature. In other words, the molecules incident upon a surface are not fully accommodated to the surface temperature.

Although no complete knowledge of the interaction process exists, it is possible to physically measure accommodation coefficients. However, due to the number of variables involved in the measurements, results often vary from one experiment to another, for investigators are unable to reproduce exactly the same combination of variables under which measurements have been made.

Of the many techniques to measure the thermal accommodation coefficient, the most widely used are the conductivity cell methods used by Knudsen, Roberts, Thomas and others and described in detail by Wachman[1], and the more recent molecular beam technique described in a survey by F.C. Hurlburt.[2]

The objective of this thesis is threefold:

1. The development of a technique to measure thermal accommodation

and normal momentum accommodation coefficients.

2. The design of an apparatus such that an atomically clean surface can be maintained for the duration of a test and can achieve reproducible results.
3. The extension of an electron beam technique to a lower density limit than has previously been achieved.

CHAPTER II

## 2. Theory

### 2.1 Kinetic Theory of Gases

The following relationships which may be found in Reference 3 are helpful in understanding the application of kinetic theory to energy and momentum accommodation:

Consider a quantity $n(\underline{x},t)$, defined as the number of molecules per unit volume at position $\underline{x}$ and at time t. Consider also a quantity $f(\underline{x},\underline{\xi},t)d\xi$ which is defined as the number of molecules per unit volume at position $\underline{x}$ and at time t with velocity $\xi$ in the range $\xi_1$ to $\xi_1 + d\xi_1$, $\xi_2$ to $\xi_2 + d\xi_2$, and $\xi_3$ to $\xi_3 + d\xi_3$. $f(\underline{x},\xi,t)$ is defined such that

$$n(\underline{x},t) = \int_{-\infty}^{\infty}\int_{-\infty}^{\infty}\int_{-\infty}^{\infty} f(\underline{x},\underline{\xi},t)\, d\xi_1\, d\xi_2\, d\xi_3 \qquad (2.1.1)$$

For a stationary gas independent of position $\underline{x}$, $f(\underline{x},\xi,t)$ is the well-known Maxwellian velocity distribution function,

$$f(\xi) = \frac{n}{(\sqrt{\pi}\, c_m)^3}\, e^{-\frac{c_i c_i}{c_m^2}}; \qquad (2.1.2)$$

where $\xi_i = u_i + c_i$,

$c_i$ is the $i^{th}$ component of the random thermal velocity,

$u_i$ is the $i^{th}$ component of the macroscopic velocity,

n is the number of molecules per unit volume,

$c_m = \sqrt{2RT}$,

R is the gas constant for the gas.

The mean value of any quantity may be calculated by using the aforementioned distribution function. Let Q be any property of the gas, and let $\overline{Q}$ be the mean value of Q. $\overline{Q}$ may be determined from

$$\overline{Q} = \frac{\int Q f d\underline{\xi}}{\int f d\underline{\xi}} . \tag{2.1.3}$$

For example, the mean value of $c_1$, is given by

$$\overline{c}_1 = \frac{\int_{-\infty}^{\infty}\int_{-\infty}^{\infty}\int_{-\infty}^{\infty} c_1 f \, d\underline{\xi}}{\int_{-\infty}^{\infty}\int_{-\infty}^{\infty}\int_{-\infty}^{\infty} f \, d\underline{\xi}} = 0 \tag{2.1.4}$$

Consider a gas with a Maxwellian velocity distribution where there is no macroscopic velocity to be considered. That is to say $\xi_i = c_i$. For ease of computation and without losing any generalities, a six-dimensional phase space coordinate system is defined by:

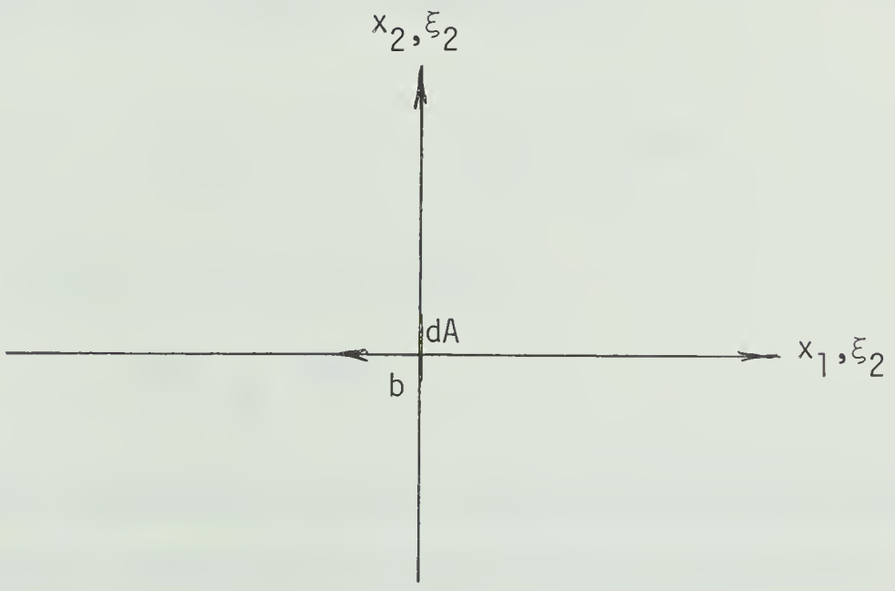


The $x_3$, $\xi_3$ coordinate is perpendicular to the $x_1$ $\xi_1$, $x_2$ $\xi_2$ plane.

For the following discussion $\xi_1 = c_1$, $\xi_2 = c_2$ and $\xi_3 = c_3$. The number of molecules crossing unit area in unit time may be derived as follows. For a molecule to cross dA in time dt it must be no further away from dA than c dt. The molecules considered are those with the $c_1$ component of velocity positive, and in the volume $\underline{dx} = c_1\ dt\ dA$. Let $N_c$ be the number of molecules crossing dA in time dt. Then,

$$N_c = \int_0^\infty \int_{-\infty}^{\infty} \int_{-\infty}^{\infty} c_1\ f\ dc_1\ dc_2\ dc_3\ dA\ dt. \qquad (2.1.5)$$

Substituting equation 2.1.2 into the above expression and performing the required integration, $N_c$ becomes

$$N_c = \frac{n\ c_m}{2\sqrt{\pi}}\ dA\ dt. \qquad (2.1.6)$$

To calculate the normal momentum crossing area dA in time dt, equation 2.1.5 is simply multiplied by the component of momentum normal to the plane dA, $mc_1$. The resulting expression is

$$P = m \int_0^\infty \int_{-\infty}^{\infty} \int_{-\infty}^{\infty} c_1^2\ f\ dc_1\ dc_2\ dc_3\ dA\ dt. \qquad (2.1.7)$$

Performing the required integration yields

$$P = \frac{1}{4}\ mn\ c_m^2\ dA\ dt. \qquad (2.1.8)$$

To calculate the amount of energy crossing dA in time dt, the number of molecules crossing dA in time dt must be multiplied by the energy carried by each molecule: $\frac{1}{2}\ mc^2$. The expression for energy

$$E = \int_0^\infty \int_\infty^\infty \int_\infty^\infty \left(\frac{1}{2} mc^2\right) c_1 \, f \, dc_1 \, dc_2 \, dc_3 \, dA \, dt, \qquad (2.1.9)$$

which, after integration, becomes

$$E = \frac{mn \, c_m^3}{2\sqrt{\pi}} \, dA \, dt. \qquad (2.1.10)$$

The average momentum and energy per molecule may be obtained from the previous expressions by dividing each equation by the number of molecules crossing dA in time dt: $N_c = \frac{n \, c_m}{2\sqrt{\pi}} \, dA \, dt$. This results in

$$\tilde{P} = \sqrt{2\pi mkT} \, , \qquad (2.1.11)$$

and

$$\tilde{e} = 2kT \, . \qquad (2.1.12)$$

From the above expressions it can be seen that the incident normal momentum is proportional to $\sqrt{T}$, whereas the energy is proportional to T.

## 2.2 Accommodation Coefficients

This thesis is concerned with the measurement of the accommodation of energy and normal momentum. Accommodation coefficients represent the efficiency with which energy or momentum is exchanged at a solid surface by a large number of incident molecules. The amount of energy or momentum actually exchanged, compared to the amount which would be exchanged in an ideal case in which the incident molecules undergo a perfectly diffuse reflection, is called an accommodation coefficient.

The energy accommodation coefficient hereafter denoted $\alpha$ is

defined by

$$\alpha = \frac{E_r - E_i}{E_s - E_i} \quad ; \qquad (2.2.1)$$

where $E_i$ is the mean energy of the molecules incident upon a surface,

$E_r$ is the mean energy of the molecules reflected from the surface,

and $E_s$ is the mean energy of the molecules if they were reflected at the same temperature as the solid.

The normal momentum accommodation coefficient, $\sigma'$, may be defined as follows, where P is the normal momentum component and the subscripts retain the same sense as in 2.2.1:

$$\sigma' = \frac{P_r - P_i}{P_s - P_i} \quad . \qquad (2.2.2)$$

To reduce the above equations to measureable forms, some knowledge of the distribution functions of the molecules must be known. The velocity distribution function corresponding to state "i" is Maxwellian, and state "s" is defined to be Maxwellian. However, some assumptions must be made concerning the distribution function of the reflected molecules in order to calculate $\alpha$ and $\sigma'$.

## 2.3 Surface Interaction Models

Several surface interaction models have been suggested in order to obtain a distribution function for the reflected molecules. These models include those discussed by Goodman[3], Logan and Stickney[4] and Epstein[5]. Hinchen and Malloy[6] have stated that although the velocity

distribution has been shown to be non-Maxwellian, "any error introduced in this assumption is probably small". For the purposes of this thesis, two models will be discussed which will lead to an experimental technique to measure the accommodation coefficients.

The first of these models is the model attributed to Maxwell. He assumed that out of all the molecules incident upon a surface, a fraction, K, were reflected with a Maxwellian velocity distribution corresponding to $T_s$, while the remaining fraction, (1 - K), were specularly reflected with a Maxwellian velocity distribution corresponding to temperature $T_i$. This implies that

$$f_r = Kf_s + (1 - K) f_i \, . \tag{2.3.1}$$

The energy $E_r$ may thus be written:

$$E_r = \int_{-\infty}^{0} \int_{-\infty}^{\infty} \int_{-\infty}^{\infty} \frac{1}{2} mc^2 \, c_1 \, f_r \, dc_1 \, dc_2 \, dc_3 \, dA \, dt.$$

Substituting for $f_r$ from equation 2.3.1, $E_r$ may be written:

$$E_r = K \int_{-\infty}^{0} \int_{-\infty}^{\infty} \int_{-\infty}^{\infty} \frac{1}{2} mc^2 \, c_1 \, f_s \, dc_1 \, dc_2 \, dc_3 \, dA \, dt + (1 - K)$$

$$\int_{-\infty}^{\infty} \int_{-\infty}^{\infty} \int_{-\infty}^{\infty} \frac{1}{2} mc^2 \, c_1 \, f_i \, dc_1 \, dc_2 \, dc_3 \, dA \, dt,$$

which becomes

$$E_r = K E_s + (1 - K) E_i,$$

Solving the above expression for K:

$$K = \frac{E_r - E_i}{E_s - E_i} \quad . \tag{2.3.2}$$

This is identical to equation 2.2.1 for $\alpha$:

$$\alpha \equiv K = \frac{E_r - E_i}{E_s - E_i} \quad .$$

The procedure is identical when deriving the expression for the normal momentum accommodation coefficient. $P_r$ may be written

$$P_r = \int_{-\infty}^{0}\int_{-\infty}^{\infty}\int_{-\infty}^{\infty} (mc_1)\, c_1\, f_r\, dc_1\, dc_2\, dc_3\, dA\, dt.$$

Upon substitution for $f_r$, $P_r$ becomes

$$P_r = K \int_{-\infty}^{0}\int_{-\infty}^{\infty}\int_{-\infty}^{\infty} (mc_1)\, c_1\, f_s\, dc_1\, dc_2\, dc_3\, dA\, dt + (1 - K)$$

$$\int_{-\infty}^{0}\int_{-\infty}^{\infty}\int_{-\infty}^{\infty} (mc_1)\, c_1\, f_i\, dc_1\, dc_2\, dc_3\, dA\, dt$$

which, upon integration, becomes

$$P_r = K\, P_s + (1 - K)\, P_i \quad .$$

Solving for K it is seen that

$$K = \frac{P_r - P_i}{P_s - P_i} \quad . \tag{2.3.3}$$

The above expression is identical to equation 2.2.2 for $\sigma'$:

$$\sigma' \equiv K = \frac{P_r - P_i}{P_s - P_i} \quad .$$

For this model $\alpha = \sigma'$.

Another suggested model involves the assumption that the velocity distribution of the reflected molecules is Maxwellian, corresponding to a temperature $T_r$ of the reflected molecules. The terms $P_r$ and $E_r$ may be written as follows:

$$P_r = \int_{-\infty}^{0} (mc_1)\, c_1\, f_r\, dc_1\, dc_2\, dc_3\, dA\, dt,$$

and

$$E_r = \int_{-\infty}^{0}\int_{-\infty}^{\infty}\int_{-\infty}^{\infty} (mc^2)\, c_1\, f_r\, dc_1\, dc_2\, dc_3\, dA\, dt.$$

$P_r$ and $E_r$ may be interpreted as representing the momentum and energy crossing an area dA in time dt from a gas in equilibrium at temperature $T_r$. Assuming that there is no accumulation of gas at the surface, an equation of continuity may be written,

$$N_{c\ \text{incoming}} = N_{c\ \text{receding}},$$

$$\frac{n_i\, c_{m_i}}{2\sqrt{\pi}} = \frac{n_r\, c_{m_r}}{2\sqrt{\pi}} = \frac{n_s\, c_{m_s}}{2\sqrt{\pi}}.$$

Using expressions 2.1.11 and 2.1.12 for the mean momentum and energy per molecule crossing a surface, and multiplying these expressions by $N_c$, $\sigma'$ and $\alpha$ may be written in terms of temperatures:

$$\sigma' = \frac{\sqrt{T_r} - \sqrt{T_i}}{\sqrt{T_s} - \sqrt{T_i}}\ ; \qquad (2.3.4)$$

$$\alpha = \frac{T_r - T_i}{T_s - T_i}. \qquad (2.3.5)$$

Clearly, these two assumptions for the velocity distribution yield different results. In the case of Maxwell's assumption, it was shown that $\alpha = \sigma'$; whereas, in the second model, $\alpha \neq \sigma'$. Results of other investigations show that in general, $\alpha \neq \sigma'$, and the reflection of molecules tends to be more diffuse than specular. The second model, which assumes that the reflected molecules have a Maxwellian distribution of velocities at a temperature $T_r$, will be used to evaluate experimental data.

## 2.4 Electron Beam Measurements

The electron beam technique used to measure the number density of molecules in a rarefied gas is an extension of a technique developed by E.O. Gadamer[7], E.P. Muntz[8], D.J. Marsden[9], and others at UTIAS.

In the present work, the range of measurements was extended to measure the density of nitrogen gas at lower densities than had yet been investigated.

The theory of electron beam density measurements may be found in the previously mentioned references and is presented here. Light output I from electron beam-excited fluorescence is given by the equation,

$$I = K n \Phi ; \qquad (2.4.1)$$

where $n$ = number density of the gas,

$\Phi$ = fluorescent light yield,

$K$ = constant which groups the factors that must be kept constant during a calibration.

The fluorescent light yield $\Phi$ is given by

$$\Phi = \frac{1}{1 + \frac{n}{n_q}} \quad , \tag{2.4.2}$$

where, for constant gas temperature,

$$\Phi = \frac{1}{1 + \frac{P}{P_q}} \quad ; \tag{2.4.3}$$

in which case, P is the operating pressure and $P_q$ is a constant, experimentally determined, reference pressure.

Light is produced by spontaneous emission from an excited electronic state of the nitrogen ion, which is reached from the ground state of the $N_2$ molecule by excitation and ionization due to a collision with a high-energy beam electron. A balance between the rate at which neutral molecules are raised to the excited state, and the rate at which the excited state is depopulated is given by,

$$F \cdot n = n' A_{mn} + 2n' n \sigma^2 \sqrt{4\pi RT} \quad ; \tag{2.4.4}$$

where $F$ = fraction of n excited by the electron beam/sec.,

$n$ = number density of the gas,

$n'$ = number density of the molecules in the excited state at any instant,

$A_{mn}$ = Einstein's spontaneous emission probability,

and $2n\, n' \sqrt{4\pi RT}$ = the collision rate per unit volume between the excited n' molecules and the n molecules. It represents the loss rate due to collisions of

excited molecules which would otherwise have given off a photon of light in making a transition to the ground state.

At higher densities, this second term on the right-hand side is significant and represents the quenching of the light output. $\sigma$ represents the collision-quenching diameter. The light output I is also written,

$$I = n' \, hc \, \nu \, A_{mn} \, . \tag{2.4.5}$$

Solving for n' from 2.4.4,

$$n' = \frac{F \, n}{(A_{mn} + 2n \, \sigma^2 \sqrt{4\pi RT})} \, , \tag{2.4.6}$$

and

$$I = \frac{F \, n \, hc \, \nu \, A_{mn}}{A_{mn} + 2n \, \sigma^2 \sqrt{4\pi RT}} \, . \tag{2.4.7}$$

Comparing equation 2.4.7 with 2.4.1 and having the expression for $\Phi$ substituted, the analogous terms yield

$$n_q = \frac{A_{mn}}{2\sigma^2 \sqrt{4\pi RT}} \, ; \tag{2.4.8}$$

in which $n_q$ has the dimension of number density. For nitrogen at room temperature, Reference (11) gives $n_q = 10^{17}$ per cm.$^3$ and $A_{mn} = 10^7$ per second. If the operating pressure is $10^{-3}$ torr and $n \approx 3.3 \times 10^{13}$, then

$$\Phi = \frac{1}{1 + \frac{3.3 \times 10^{13}}{10^{17}}} \approx 1 \, .$$

For pressures of $10^{-3}$ torr and below $\Phi \approx 1$; leaving I = Kn. This implies that the light output is a function of the gas density.

In the spectrum of nitrogen excited by the electron beam, the $N_2^+$ (0,0) band with a band head at 3914 Angstroms is the most intense. This is the band which has been selected for use in this investigation. A calibration is necessary to determine a value for the constant K for this particular apparatus. The calibration groups the following factors together:

a) Fluorescent light yield;

b) The dependence of the total inelastic collision cross section on electron energy;

c) Electron beam current;

d) The varying transparencies of windows, lenses, and so on, and use of a filter;

e) Spectral sensitivity characteristic of the photomultiplier used;

f) The photomultiplier high voltage (which controls the overall sensitivity);

g) The angular aperture of the collecting lens;

h) The length and width of the electron beam section, from which the light is received by the photomultiplier.

Once the calibration has been established, all of these quantities and properties must be kept constant. In addition to the above, gauges and light baffles must not be moved after calibration, since a great deal of care must be taken to keep the background light to a minimum. The calibration technique and results are outlined in sections 4.1 and 5.2.

## 2.5 Measurement of Translational Energy and Normal Momentum Accommodation Coefficients

Values for $\alpha$ and $\sigma'$ may be found by the technique now to be described, making the assumption that the reflected molecules have a Maxwellian velocity distribution.

Consider the schematic diagram (Fig. 2) in which molecules, after being reflected from a solid surface, pass through and into a region of lower gas density. An electron beam which passes through a point P just below the orifice is used to measure the number density at point P by the electron beam technique previously described.

For a particular set of conditions in the test chamber, the number of molecules passing through the test chamber orifice has a given value, $N_{c_r}$, which is independent of the crystal temperature, $T_s$, and depends only on $n_i$ and $T_i$. This results in the number density at point P having a value, n. If $N_{c_r}$ remains constant, but there is an increase in the speed of the molecules crossing the orifice due to $T_r$ being greater than $T_i$, the number density at point P will be less by a small amount due to the smaller amount of time each molecule spends in the small volume located at P.

We may write the number density n of the molecules at point P as

$$n = n_a + n_b \; ; \qquad (2.5.1)$$

where $n_a$ is the contribution to the number density at point P by the molecules coming through the orifice in the solid angle $d\omega_1$,

and $n_b$ is the contribution to the number density at point P by the molecules in the remaining solid angle, $4\pi - d\omega$.

If $n_r$ is the number density of the molecules reflected from the solid surface, then

$$n_a = n_r \frac{d\omega}{4\pi} \quad ; \tag{2.5.2}$$

and if $n_c$ is the number density of the molecules in the background gas, then

$$n_b = n_c(1 - \frac{d\omega_1}{4\pi}) \quad . \tag{2.5.3}$$

Let $\frac{d\omega_1}{4\pi} = G_1$, and $(1 - \frac{d\omega_1}{4\pi}) = G_2$; then,

$$n = n_r G_1 + n_c G_2 \quad ,$$

such that $n_r$ becomes

$$n_r = \frac{n - n_c G_2}{G_1} \quad . \tag{2.5.4}$$

It has been shown in Equations 2.3.4 and 2.3.5 that $\alpha$ and $\sigma'$ may be written

$$\alpha = \frac{T_r - T_i}{T_s - T_i} \quad ,$$

and

$$\sigma' = \frac{\sqrt{T_r} - \sqrt{T_i}}{\sqrt{T_s} \quad \sqrt{T_i}} \quad .$$

Employing the continuity equation,

$$\frac{n_i \, c_{m_i}}{2\sqrt{\pi}} = \frac{n_r \, c_{m_r}}{2\sqrt{\pi}} \quad ,$$

it can be shown that

$$\frac{n_i}{n_r} = \frac{\sqrt{T_r}}{\sqrt{T_i}}$$

$$\left(\frac{n_i}{n_r}\right)^2 = \frac{T_r}{T_i} \quad . \tag{2.5.5}$$

Using the above expressions with those for $\alpha$ and $\sigma'$ it is seen that

$$\alpha = \frac{\left(\frac{n_i}{n_r}\right)^2 - 1}{\frac{T_s}{T_i} - 1} \tag{2.5.6}$$

and

$$\sigma' = \frac{\left(\frac{n_i}{n_r}\right) - 1}{\sqrt{\frac{T_s}{T_i}}} \quad .$$

A value for $d\omega_1$ may be calculated from the geometry of the experimental apparatus. Consider Fig. 4, where d is the perpendicular distance from the plane of the orifice to the test volume at point P, and $r_o$ is the radius of the orifice. The solid angle $d\omega_1$ is calculated as follows:

$$d\omega_1 = \int_0^{2\pi} \int_0^{r_o} \frac{r \, dr \, d\theta}{r^2 + d^2} \quad ,$$

$$d\omega_1 = \pi \ln \left(\frac{r_o^2 + d^2}{d^2}\right) \quad . \tag{2.5.7}$$

Using as values $r_o$ = 1.04 mm and d = 11.05 mm, $d\omega_1$ is 0.0274 steradians.

$G_1$ and $G_2$ may be calculated and become

$$G_1 = 0.00218$$

and

$$G_2 = 0.99782 \approx 1.0 \quad .$$

If the value for $n_r$ in Equation 2.5.4 is substituted into the expressions for $\alpha$ and $\sigma'$, the result is

$$\alpha = \frac{\left(\frac{2.18 \times 10^{-3} n_i}{n - n_c}\right)^2 - 1}{\frac{T_s}{T_i} - 1} \quad , \qquad (2.5.8)$$

and

$$\sigma' = \frac{\left(\frac{2.18 \times 10^{-3} n_i}{n - n_c}\right) - 1}{\sqrt{\frac{T_s}{T_i}} - 1} \quad . \qquad (2.5.9)$$

## 2.6 Surface Conditions

Probably the most important factor to be considered when measuring accommodation coefficients is the condition of the surface of the material being tested. For example, surfaces which have adsorbed gas layers tend to exhibit a diffuse reflection, while a surface with little or no adsorbed gas particles may exhibit a nearly specular reflection. Wachman[10] has shown the effect of adsorbed gas molecules on a surface and has demonstrated that the value of an accommodation coefficient may decrease by a factor of as great as ten for a clean surface, compared

to one with an adsorbed layer of gas molecules.

To compare measurements of thermal accommodation coefficients, it is necessary to specify not only the type of surface and gas but also the condition of the surface. The exact degree of contamination is very difficult to specify, which leaves the alternative of making all measurements on a reproducibly clean surface. This surface should be free of all but a few per cent of a single monolayer of foreign atoms; in other words, an atomically clean surface. The test apparatus must be designed with this high degree of cleanliness in mind. Once a clean surface is obtained, it may be possible to modify it with known types and amounts of contaminants.

In practice, many difficulties arise when trying to obtain an atomically clean surface, because most metals react chemically with vacuum system gases such as $N_2$, $O_2$, $H_2O$, $CO$, $CO_2$, and some hydrocarbons, which are commonly adsorbed on surfaces in vacuum systems. These gases are being constantly desorbed from the walls of the vacuum system to form the gas load which limits the ultimate pressure reached. This limiting gas load may be lowered by a thorough bakeout of the vacuum system, which decreases the rate of desorption of gases from the vacuum system walls.

It is seen[11] that some surfaces will chemisorb certain gases, whereas other surfaces are not affected by the same gas. For example, tungsten and molybdenum will chemisorb all of the aforementioned gases, whereas platinum will chemisorb all of the gases with the exception of nitrogen.

If nitrogen is being used as the test gas, and nitrogen will chemisorb on the surface at room temperature, one must be content to measure the accommodation coefficient of $N_2$ on a surface upon which $N_2$ has already adsorbed. It is necessary, however, to reduce the degree of contamination caused by the adsorption of the other molecules in the system which, for this purpose, may be called impurity gases.

A practical method to reduce the degree of contamination would be to reduce the partial pressure of the impurity gases such that the time taken to form a monolayer of the impurity gas is longer than the time to conduct a test. For example, if the time necessary to conduct an experiment is 30 minutes, it is possible to calculate what the partial pressure of the impurity gases must be so that a monolayer will not form in 30 minutes.

The number of molecules in a monolayer is about $10^{15}$ per square centimeter, and the number of molecules striking one square centimeter per second is $N_c = 3.52 \times 10^{22} \frac{P}{\sqrt{MT}}$; where P is the pressure in torr, M is the molecular weight, and T is the temperature of the gas in degrees Kelvin. If it is assumed that an approximate weight of an impurity gas is 30, then if each molecule striking the surface sticks to it, the background pressure of the impurity gas can be no greater than $1.5 \times 10^{-9}$ torr. This means that for a test run time of less than 30 minutes, the partial pressure of the background must be of the order of $10^{-9}$ torr. If the working pressure of the gas is to be $10^{-3}$ torr, the impurities in the gas must be less than one part per million. The gas being admitted to the vacuum system, therefore must have impurities of less than one part per million. If a commercially available gas is

not pure enough, the gas may be cleaned during admission by selective gettering. Rhodium, for example, will chemisorb all gases with the exception of nitrogen, and nickel will chemisorb all gases with the exception of nitrogen and methane. This means that nickel or rhodium may be used to clean the gas as it is admitted to the vacuum system. Any water vapour or other condensable materials may be removed by a cold trap in the inlet line.

A clean test surface is produced by several methods, such as ion bombardment, deposition of the test surface by a sublimation process, or by high-temperature resistive heating to evaporate condensed gas layers or other contamination. If silicon is heated to 1530°K, it is sufficient to thoroughly degas the surface so that a clean surface measurement may be made. Tungsten requires a degas temperature of 2400°C and molybdenum requires a temperature of 1760°C. With careful control of conditions, it is possible to produce an atomically clean surface for a limited time.

CHAPTER III

# 3. Experimental Apparatus

## 3.1 The Vacuum System

The vacuum system was constructed using stainless steel wherever possible, for it gives large systems the capability of being rugged, dependable and easily bakeable. All joints were welded using an inert gas welding technique to prevent oxidation and bubbling of the metal, thus preventing virtual leaks. All demountable vacuum joints were made with Varian Conflat-type flanges, using bakeable copper gaskets. The vacuum system was bakeable to 450°C.

The oven which enclosed the aforementioned portion of the vacuum system was made of a commercially available insulating material, and lined with aluminum foil. Bake out temperatures were of the order of 300°C.

For the purposes of explanation, the different chambers of the vacuum system may be labelled A, B, and C (see Fig. 2). Chamber A is the chamber in which the gas-surface interaction takes place. It is the chamber with the highest working pressure: approximately $5 \times 10^{-4}$ torr. This chamber contains the Baritron gauge, the Bayard-Alpert gauge, the gas inlet, the thermocouples to measure $T_i$, and the test surface. In chamber B there is the electron beam measuring apparatus, in which the background pressure should be of the order of $1 \times 10^{-8}$ torr. This chamber also contains the light baffles and the lens for the photo-multiplier measurements. Chamber C is the pumping chamber, containing the triode ion pump and one titanium sublimation pump.

Chambers A and B are connected by a 2.08 mm diameter orifice as

well as a 1.5" diameter bypass tube which, when sealed, causes all of the flow to pass through the orifice. The conductance of the orifice, C, is 0.37 litres per second, and the effective pumping speed, s, from chamber B, is approximately 1900 litres per second. From molecular flow theory,

$$P_B = \frac{C}{C + s} P_A = 1.95 \times 10^{-4} P_A .$$

Thus, when $P_A = 10^{-4}$ torr, $P_B = 1.95 \times 10^{-8}$ torr .

## 3.2 Pumps

During bakeout, the entire vacuum system was pumped by a 4 litre per second roughing pump. A liquid nitrogen cold trap was used to prevent diffusion of oil from the roughing pump to the vacuum system. The roughing pump held the system pressure at about 10 microns during bakeout.

A 100 litre per second triode ion pump and a titanium sublimation pump were used to obtain the ultra-high vacuum conditions required for testing. Chamber C, which contains the titanium sublimation pump, is cooled by an inner shell containing liquid nitrogen to prevent the titanium sublimation filament from heating the vacuum chamber, and to increase the pumping efficiency of the titanium sublimation deposits.

During the electron beam calibration, only the triode ion pump was used, because high pumping speed was not required. But, during the measurements of accommodation, the titanium sublimation was the primary pump, the purpose of the ion pump being to remove the inert

gases not pumped by the titanium films.

## 3.3 Pressure Gauges

A Varian partial pressure gauge capable of measuring both total pressure and partial pressure was used to monitor the partial pressure of the nitrogen gas during the electron beam calibration. This gauge was used to indicate the condition of cleanliness of the vacuum system, in order to make sure that the partial pressures of the impurity gases were below the tolerable upper limit. This gauge was used in chamber C. A Bayard-Alpert gauge was used in chamber A to monitor the pressure during the test surface cleaning period. An MKS Baratron Model 90H-3 pressure transducer was used to measure the pressure in chamber A during the test. This pressure was then related to the number density, $n_i$, to be used in expressions 2.5.8 and 2.5.9. The Baratron capacitance transducer is a direct-pressure measuring device. There is no heating due to filaments to cause unwanted outgassing of the surrounding structure, and no conversion factor is required to take account of the relative ease of ionization of different gases present. This gauge is used as a reference transducer for the automatic pressure controller. This instrument had to be zeroed by reducing the test gas pressure to zero. This had to be done after approximately 20 minutes of operation to keep the instrument drift within an acceptable limit of about 2 per cent.

A pirani gauge was used to monitor the pressure during bakeout and during the pumping with the roughing pump, and a thermocouple gauge was used to measure the pressure in the inlet pressure limiter.

## 3.4 Temperature Measurement and Control

Resistive heating was used to bake the test surface to produce a clean surface for the test measurements.

A Huggins Mark 1 infrascope radiation thermometer was used to monitor the test surface temperature and was aimed at the test surface through a viewing port in chamber A (Fig. 2). The emissivity control on the instrument must be set for each material used as a test surface. The radiation emitted must be in the spectral range 1.8 to 2.7 microns. A ten per cent change in the value of the emissivity setting when measuring the temperature of a tungsten filament would cause a change of about three per cent in the temperature reading. If a mean value of emissivity is chosen for the aforementioned spectral range, the errors involved in the measurement of the temperature of the test surface should be small.

The temperature of the incident gas molecules was assumed to be equal to the wall temperature in chamber A, which was measured using chromel-alumel thermocouples and a suitable millivolt readout device. The temperature of the walls in chamber A was kept uniform by circulating water through a water jacket enclosing the chamber.

## 3.5 Pressure Control and Gas Admittance

The output signal from the Baratron pressure transducer was fed into the control unit of a Granville-Phillips automatic pressure controller. This controller operates by matching an output voltage from

a pressure transducer to a preset reference voltage on the automatic pressure controller. The signal difference regulates the opening and closing of the servo-driven leak valve, thus controlling the system pressure.

The servo-controlled leak valve was not able to control the pressure when the inlet gas was supplied at atmospheric pressure. This was due to the very small pumping speed through the orifice between chambers A and B when the bypass valve was closed. This situation was remedied by using an intermediate chamber in the inlet line so that the inlet pressure to the leak valve was only about 2000 microns.

The commerically available $N_2$ gas being admitted to the system is further cleaned by using a selective getter trap as well as a cold trap to remove the condensable impurities. In this system, a vapour-deposited nickel film was used to remove the impurities without, however, its reacting with the nitrogen gas.

## 3.6 Electron Gun and Photomultiplier

The electron gun used in this experiment was a Phillips 902-564, one which is normally used in a television picture tube. It was mounted inside a glass tube which is attached to a Varian con-flat flange by a glass-to-metal seal. The aiming system for the electron gun was designed so that rotational and transverse motions were obtainable. It was aimed through a 1.5 millimeter diameter collimating hole such that the electron beam was well-defined when passing through the measuring volume at point P in chamber B. The lens voltages on the

electron gun were obtained from a voltage divider chain, a circuit of which is shown in Fig. 5, and the power for the gun was supplied by an N.J.E. 0-30 KV, 0-2.5 ma power supply. The normal operating voltage was 10 KV. The maximum operating current was 2.5 ma, of which a portion is the actual beam current. This beam current was monitored by a milli-ammeter in line with the collector cup to ground.

An EMI 9502S photomultiplier was used to measure the fluorescent light output from the excited nitrogen molecules. When the cathode voltage is -1000 volts, the dark current of this tube was $6 \times 10^{-12}$ amps at room temperature, with a fluctuation of $\pm .5 \times 10^{-12}$ amps. The power supply for the photomultiplier is a Fluke Model 410B 0-2.1 KV which has a high degree of regulation.

The signal produced by the electron beam-excited luminescence was very small, making it necessary to eliminate any stray light from the surroundings, such as wall fluorescence, glowing filaments, and light passing into the system through glass ports. The most effective way of eliminating the unwanted background light is by the use of a narrow-band pass filter. A Bausch and Lomb interference filter, having a maximum transmission of 35 per cent at 3900 Angstroms, and a half width of 140 Angstroms, was used. Light baffles were also used to reduce the background light. The photomultiplier was mounted on a traversing mechanism in order to adjust its position to look at the maximum light intensity. The photo current was measured by using a Keithly Instruments 610B electrometer.

# CHAPTER IV

## 4. EXPERIMENTAL PROCEDURE

### 4.1 Electron Beam Calibration

Before any accommodation measurements can be made, the electron beam density-measurement apparatus has to be calibrated. This was done, keeping in mind that further changes in the apparatus could not be tolerated after calibration. The calibration took the form of a plot of photo current output I versus the partial pressure of nitrogen in the electron beam chamber at point P (see Fig. 8 for the calibration). The calibration was accomplished by a static test measurement of the partial pressure of nitrogen at point P, recording the corresponding photo current output.

The partial pressure of nitrogen at point P was made up of two parts, the contribution by the molecules coming through the orifice from chamber A, and the contribution from the molecules in chamber B. The analysis is as follows:

Let $$P_{N_2} = P_{N_{2a}} + P_{N_{2b}} \quad ; \qquad (4.1.1)$$

where $P_{N_{2a}}$ is the contribution to $P_{N_2}$ from the molecules coming through the orifice,

and $P_{N_{2b}}$ is the contribution from the molecules in chamber B.

Following the same analysis as in section 2.5,

$$P_{N_{2a}} = P_{N_{2i}} \frac{d\omega_1}{4\pi} \quad ; \qquad (4.1.2)$$

where $P_{N_{2i}}$ is the partial pressure of nitrogen gas in chamber A,

and

$$P_{N_{2b}} = P_{N_{2B}} \left(1 - \frac{d\omega_1}{4\pi}\right) \quad ; \qquad (4.1.3)$$

where $P_{N_{2B}}$ is the partial pressure of nitrogen in chamber B. Letting

$\frac{d\omega_1}{4\pi} = G_1$ and $1 - \frac{d\omega_1}{4\pi} = G_2$,

$$P_{N_2} = P_{N_{2i}} (G_1) + P_{N_{2B}} (G_2) \; .$$

There are two methods which can be used to calibrate the apparatus. The first of these involves opening the valve interconnecting chambers A and B, thus increasing the contribution to the partial pressure at point P by the molecules in chamber B. In this case, the main contribution comes from the molecules in chamber B, and a calibration may be accomplished for pressure ranges covering at least 2 decades. The other method is to close the valve connecting chambers A and B. This results in the main contribution coming from the molecules passing through the orifice. In this case, the contribution from the molecules in chamber B is small. Of these two methods, the second was chosen because it more closely simulated the conditions under which the accommodation measurements are conducted.

The electron beam could not be used simultaneously with the partial pressure gauge due to the magnetic field associated with the partial pressure gauge magnet, and hence plot of partial pressure of nitrogen versus total pressure was needed to related the total pressure measured to the partial pressure of nitrogen. The partial pressure values could

then be correlated to the total pressure readings when the electron beam was run. Figure 6 shows a typical partial pressure traverse from which the partial pressure of nitrogen may be calculated. This is done as follows:

$$P_{N_2} = \frac{\text{Peak height of } N_2^+}{\Sigma \text{ All peak heights}} \times P_{\text{total}}$$

The electron beam calibration was run holding the following parameters constant:

1. Electron beam voltage: 10 KV;
2. Heater current for filament: 0.66 amps;
3. Total current: 2.0 ma;
4. Beam current: 0.55 ma.

As the pressure in chamber B was increased, a focussing effect due to space charge neutralization by ions formed would cause an increase in the electron beam current. Since the light output caused by gas fluorescence depends on the electron beam current, this beam current must be kept constant. This was accomplished by electronically defocussing the beam to compensate for the focussing effect due to space charge neutralization.

The contribution to the photo current by the background light was also found to be dependent on pressure. This contribution was found by moving the photomultiplier slit to either side of the electron beam image and recording the corresponding photo current. The background current corresponding to the particular pressure was subtracted from the total photo current readings to determine the amount dependent on the nitrogen density at point P.

The way in which the data was reduced is indicated by the following example: $P_i = 6.5 \times 10^{-4}$ torr, and $I = 7.2 \times 10^{-11}$ amps, are typical readings obtained during a calibration run. From section 2.5 it was seen that $G_1 = \frac{d\omega_1}{4\pi}$ was equal to $2.18 \times 10^{-3}$. The resulting contribution to the pressure at point P was $2.18 \times 10^{-3} P_i = 1.46 \times 10^{-6}$ torr. Knowing that $P_B = 1.95 \times 10^{-4} P_i$ from the pumping speed and conductance relationships, and knowing $G_2 \approx 1.0$, gives the contribution to the pressure at point P from the molecules in chamber B as $0.13 \times 10^{-6}$ torr. Using Fig. 7, the total pressure at point P, $1.56 \times 10^{-6}$ torr, may now be converted to the partial pressure of nitrogen. This pressure, $P_{N_2}$, is $9.2 \times 10^{-7}$ torr. The corrected photo current is used in conjunction with the partial pressure of nitrogen. This is found by subtracting the background current contribution from the measured photo current. Thus $3.2 \times 10^{-11}$ amps background current must be subtracted from $7.2 \times 10^{-11}$ amps, leaving the corrected photo current $4.0 \times 10^{-11}$ amps. This value, with the partial pressure of nitrogen, is shown plotted on Fig. 8.

## 4.2 Procedure for Measurement of Accommodation Coefficients

Having completed the calibration, the apparatus is now ready for measuring accommodation coefficients. Although no measurements of accommodation were made, the procedure to be followed is described below.

The target is cleaned by flashing it to a high temperature to evaporate adsorbed gases and oxides. The bypass valve is kept open during this degassing process to allow the desorbed gases to be pumped away. After having cleaned the target surface, the bypass valve connecting

chambers A and B is closed and the test may commence. The same conditions under which the calibration was done must be adhered to when a measurement of accommodation is made.

With water running in the watercooled jacket surrounding chamber A, the pressure is brought up to the operating range by the automatic pressure controller. The photo current output is now measured and, after suitable dark current corrections, may be correlated to the number density of the nitrogen gas at point P. The temperature of the surface is measured using the radiation thermometer, while the incident gas temperature is assumed to be the same as that of the chamber walls measured using chromel-alumel thermocouples. This data may be used in conjunction with the relationships in section 2.5 to determine the accommodation coefficients.

# CHAPTER V

## 5. DISCUSSION

### 5.1 Analysis of Errors

Although accommodation measurements have not yet been made with the apparatus, the analysis of expected errors involved is presented. The expression for $\alpha$, found in section 2.5,

$$\alpha = \frac{(\frac{G_1 n_i}{n - n_c})^2 - 1}{\frac{T_s}{T_i} - 1} ,$$

is analysed in terms of the quantities to be determined experimentally. These quantities are $G_1$, $n_i$, $n$, $n_c$, and $T_s/T_i$. The errors involved are not available, but, used as follows, they will yield a representation of the accuracy of the experiment.

The error in $\alpha$, $\Delta\alpha$, is

$$\Delta\alpha = \frac{\partial\alpha}{\partial G_1} \Delta G_1 + \frac{\partial\alpha}{\partial n_i} \Delta n_i + \frac{\partial\alpha}{\partial n} \Delta n + \frac{\partial\alpha}{\partial n_c} \Delta n_c + \frac{\partial\alpha}{\partial \frac{T_s}{T_i}} \Delta\frac{T_s}{T_i} \qquad (5.1.1)$$

made up of

a) $\frac{\partial\alpha}{\partial G}$ which is the sensitivity of $\alpha$ to an error in $G_1$, and is

$$\frac{\partial\alpha}{\partial G_1} = \frac{2 n_i^2 G_1}{(n - n_c)^2(\frac{T_s}{T_i} - 1)} ; \qquad (5.1.2)$$

b) The sensitivity of $\alpha$ to an error in $n_i$ is

$$\frac{\partial \alpha}{\partial n_i} = \frac{2\, G_1^{\,2}\, n_i}{(n - n_c)^2 \left(\frac{T_s}{T_i} - 1\right)} \quad ; \qquad (5.1.3)$$

c) For an error in n,

$$\frac{\partial \alpha}{\partial n} = \frac{-2(G_1 n_i)^2}{(n - n_c)^3 \left(\frac{T_s}{T_i} - 1\right)} \quad ; \qquad (5.1.4)$$

d) For an error in $n_c$,

$$\frac{\partial \alpha}{\partial n_c} = \frac{2(G_1 n_i)^2}{(n - n_c)^3 \left(\frac{T_s}{T_i} - 1\right)} \quad ; \qquad (5.1.5)$$

e) and for an error in $T_s/T_i$ the sensitivity is

$$\frac{\partial \alpha}{\partial \left(\frac{T_s}{T_i}\right)} = \frac{-\left[\left(\frac{G_1 n_i}{n - n_c}\right)^2 - 1\right]}{\left(\frac{T_s}{T_i} - 1\right)^2} \qquad (5.1.6)$$

These formulae together with estimated values of the individual errors will yield the overall experimental error.

To estimate the size of experimental error to be expected, the calibration curve will indicate typical scatter from which the magnitude of random deviation errors may be estimated. The following values of quantities to be measured are considered to be typical.

$$n_i = 4.95 \times 10^{12}/cm^3 \quad ,$$

$$n = 1.35 \times 10^{10}/cm^3 \quad ,$$

$$n_c = 1.78 \times 10^{9}/cm^3 \quad ,$$

$$G = 2.18 \times 10^{-3} \quad ,$$

$$\frac{T_s}{T_i} = 1 \quad .$$

Probable errors in the experimentally determined quantities are assumed to be:

$$\Delta G_1 = 0.005\ G_1 \quad ,$$

$$\Delta n_i = 0.02\ n_i \quad ,$$

$$\Delta n = 0.02\ n \quad ,$$

$$\Delta n_c = 0.02\ n_c \quad ,$$

$$\Delta \frac{T_s}{T_i} = 0.01\ T_s/T_i \quad .$$

Using expressions 5.1.2 to 5.1.6 together with the estimated accuracy of the individual measurements we find

$$\Delta\alpha G_1 = 0.0043 \quad ,$$

$$\Delta\alpha n_i = 0.0172 \quad ,$$

$$\Delta\alpha n = 0.0198 \quad ,$$

$$\Delta\alpha n_c = 0.0026 \quad ,$$

$$\Delta\alpha \frac{T_s}{T_i} = 0.0006 \quad ;$$

leading to a total error of

$$\Delta\alpha = 0.0445 \quad .$$

This implies that with careful measurements, the total scatter in experimental results may be held to within 4.5 per cent.

The results which have been obtained for the electron beam calibration are valid as an accommodation measurement if the accommodation coefficient is unity. Using expression 2.5.8 for $\alpha$, it is possible to estimate the change in n for an observed change in $\alpha$ Dealing in terms of pressures which correspond to the number densities of 2.5.8 for $\alpha = 1$, $P_i = 5 \times 10^{-4}$, $P_c = .16 \times 10^{-6}$, and $P = 1.2 \times 10^{-6}$. Assuming that $T_2/T_1 \approx 2$ and $\alpha = 1/2$, P is found to be $1.05 \times 10^{-6}$. This value is in the range covered by the electron beam calibration.

## 5.2 Electron Beam Analysis

The photomultiplier optics are shown in a schematic diagram, Fig. 3. A lens of focal length 53 mm was used, and an object distance of 96 mm required that the image distance be 120 mm. The resulting magnification is 1.25.

The electron beam width may be estimated from available geometric data such as the photomultiplier cathode slit size and optical magnification, together with a traverse of the photomultiplier slit across the image of the beam. The edges of the beam are somewhat indefinite due to its cylindrical shape and to a halo caused by scattered electrons.

If it is assumed that the beam is of cylindrical shape and the slit is rectangular, the traverse can be represented by a traverse of a rectangular slit across a circular cross section, plotting the area seen through the slit as a function of the slit position.

The following analysis represents the theoretical traverse:

$$I = \lambda A \ ;$$

where I is the arbitrary intensity measured as photo current in amps,

$\lambda$ is a constant to correlate the results of the theoretical traverse to the actual traverse,

and A is the area as seen through the slit.

A may be written as a function of the position of the slit:

$$A = R^2\left(\cos^{-1}\left(\frac{r - \frac{\alpha}{2}}{R}\right) - \frac{\left(r - \frac{\alpha}{2}\right)\sqrt{R^2 - \left(r - \frac{\alpha}{2}\right)^2}}{R^2}\right) \ , \qquad (5.2.1)$$

for $R - \frac{\alpha}{2} < r < R + \frac{\alpha}{2}$ ,

and

$$A = R^2\left(\cos^{-1}\frac{\left(r - \frac{\alpha}{2}\right)}{R} - \cos^{-1}\frac{\left(r + \frac{\alpha}{2}\right)}{R} - \frac{\left(r - \frac{\alpha}{2}\right)\sqrt{R^2 - \left(r - \frac{\alpha}{2}\right)^2}}{R^2} + \frac{\left(r + \frac{\alpha}{2}\right)\sqrt{R^2 - \left(r + \frac{\alpha}{2}\right)^2}}{R^2}\right) \ ,$$

for $0 < r < R - \frac{\alpha}{2}$ ;

where R = assumed radius of beam,

$\alpha$ = slit width,

and r = position of center of slit from center of circle.

The results of this theoretical traverse are shown in Fig. 9, with the actual traverse reduced to the plane of the electron beam superimposed. It was assumed that the electron current was constant across the beam

and that the beam was well defined. This assumption does not appear to be correct. However, the best fit curve appeared to be the assumed 1.5 mm diameter. The beam may be considered to be 1.5 mm diameter if the discrepancy is considered to be due to slight beam divergence near the edges, the halo of light surrounding the beam, and an inefficiency in the optical lens.

It was shown in section 2.4 that at pressures below $10^{-3}$ torr, $I = Kn$. The overall sensitivity of the electron is $\frac{dI}{dn} = K$, and is an important factor when trying to extend the density measurements to lower ranges. Factors which affect the sensitivity include adsorption and reflection at lenses and windows, the aperture of the lens (the quantity of light collected), electron beam current, and voltage. More difficult to predict, however, are the effects on sensitivity caused by the background signal due to extraneous light from wall fluorescence caused by high energy electrons striking parts of the apparatus. The overall sensitivity may be determined as follows. Consider the equation,

$$I = Kn .$$

Taking logs of both sides,

$$\ln I = \ln n + \ln K,$$

or, for constant temperature, $\ln I = \ln P_{N_2} + \ln K_1$ .

This implies that when the results are plotted on log-log paper, the slope of the curve must be unity. The intercept when $P_{N_2}$ is unity will yield the overall sensitivity in amps/torr. The calibration curve, Fig. 8, yields an overall sensitivity, $K_1$, of $4.1 \times 10^{-5}$ amps/torr. An

upward shift in this curve would imply a greater sensitivity.

On the same graph is another curve which shows a calibration of the apparatus before major changes were incorporated. The observed increase in sensitivity needs some qualification. Before the changes were made, a different photomultiplier tube, a larger cathode slit size, and different optics were used. These conditions resulted in higher background and signal currents, but the resulting signal-to-background current ratio was the same. Thus the lower density limit was almost identical in both cases.

The effective collision cross section for excitation of the nitrogen molecules to the upper state of transition by high energy electrons is an important factor for system comparison. It gives a measure of the electron-molecule interaction efficiency.

The number of collisions per second which produce a photon is given by

$$N = (n_e V_e Q)(n A_e dz) \quad ; \qquad (5.2.2)$$

where $n_e$ = number density of electrons,

$V_e$ = velocity of electrons,

$Q$ = effective collision cross section,

$n$ = number density of molecules,

$A_e$ = area of electron beam,

and $dz$ = length of electron beam being considered in measurement.

$n_e$ may be calculated from

$$n_e = \frac{i}{A_e V_e} \quad ; \qquad (5.2.3)$$

where $i$ = the electron beam current in electrons/sec.

Substitute the value for $n_e$ in equation 5.2.2, and

$$N = n\, i\, Q\, dz \quad . \tag{5.2.4}$$

N is also the number of photons produced per second.

Assuming that light is radiated equally in all directions, only a certain percentage of this light is collected by the focussing lens. Consider the lens with its diameter of 38 mm and the object distance of 120 mm. The solid angle subtended by the lens may be calculated using equation 2.5.7:

$$d\omega = \pi \ln \left(\frac{R^2 + D^2}{D^2}\right) \quad ;$$

where R is the lens radius and D is the object distance,

$$d\omega = \pi \ln \left(\frac{19^2 + 96^2}{96^2}\right) \quad ,$$

$$= 0.12 \ ,$$

therefore $$\frac{d\omega}{4\pi} = 0.0095 \ .$$

Therefore, the light collected is 0.0095 light-produced.

The light loss in the optical elements such as lens, window, and filter, may be estimated and expressed as a percentage transmittance, T. A liberal estimate for T would be approximately 0.2. The efficiency of the photomultiplier cathode E is approximately 0.15, and the photomultiplier gain, G, is of the order of $10^8$ electrons per photoelectron.

Combining these factors with equation 5.2.3,

$$I = n\,Q\,i\,dz\,\left(\frac{d\omega}{4\pi}\right)\,TEG/6.25 \times 10^{18}\ \text{amps} \quad ; \qquad (5.2.5)$$

I being the photo current measured in amps.

Typical values are $I = 5 \times 10^{-11}$ amps, $n = 3.5 \times 10^{10}$ molecules/$cm^3$, $i = 3.125 \times 10^{15}$ electrons/sec, and dz = 0.3 cm. Substituting these values in the above expression and solving for Q,

$$Q = \frac{6.25 \times 10^{18}\ I}{n\ i\ \left(\frac{d\omega}{4\pi}\right)\ dz\ TEG} \quad ,$$

$$= 3.3 \times 10^{-22}\ cm^2 \ .$$

Expression 5.2.5 is analogous to an expression which Gadamer[7] used to describe the calibration technique,

$$I = n\gamma\ \Delta s\ Ie \ ;$$

where I is the photo current,

$\Delta s$ is analogous to dz,

Ie is analogous to i,

and $\gamma$ lumps the remaining factors. $Q\ \frac{d\omega}{4\pi}\ TEG$ thus keeping i constant through a calibration, again gives us I = Kn and a means of calculating the sensitivity. It can be immediately seen how factors such as Q affect the sensitivity.

The lower pressure limit, however, is mainly dependent on the reduction of the background current such that signal-to-background ratios

are not low, 1:10 as a minimum. From this, a conservative estimate of the lower pressure limit of this technique would be $1 \times 10^{-7}$ torr.

## 5.3 Advantages

a) A large range of temperature differences between the target and the incident molecules may be used. The higher temperature results in a higher sensitivity when measuring the number density of the nitrogen molecules at point P and consequently a higher sensitivity when measuring accommodation coefficients.

b) A high target temperature allows the target to be kept in a range where very few gas molecules are adsorbed.

c) A wide range of materials may be used. Not all materials may be drawn into wire form, as is required for the conductivity cell measurements.

d) The temperature of the test surface may be measured remotely, thus eliminating thermocouple problems.

e) The number density of nitrogen is measured directly independent of any other gases which may be present.

# CHAPTER XI

## 6. CONCLUSIONS

1. The apparatus as designed will measure energy and normal momentum accommodation coefficients with scatter in experimental results of less than 4.5 per cent.
2. The apparatus will allow the tests to be carried out on a clean surface for a short-duration test, if care is taken in proper cleaning of the apparatus and the admission of the gas.
3. This technique will provide measurements using a large number of materials and a large range of temperature differences; however, the number of gases which may be used is limited.
4. The electron beam fluorescence density measurements in nitrogen may be extended to a density corresponding to $10^{-7}$ torr. The sensitivity of the calibration is $4.1 \times 10^{-5}$ amps/torr.
5. The background photo current caused by wall fluorescence and stray light is the limiting factor when extending the electron beam technique to lower densities.
6. The collision cross section for the $N_2^+$ (0,0) vibrational transition is $3.3 \times 10^{-22}$ $cm^2$.

## FOOTNOTES

1. Wachman, "Thermal", 2-12.
2. Hurlburt, "Molecular Interactions", University of California Tech Report.
3. Goodman, "Accommodation Coefficients", 85-105.
4. Logan and Stickney, "Simple Classical Model", 195-205.
5. Epstein, "Wall Boundary Condition", 1797-1800.
6. Hinchen and Malloy, "Molecular Beam", 3.
7. Gadamer, "Optical Electron Beam", 13-15.
8. Muntz, "Rotational Temperature", 20.
9. Marsden, "Energy Transfer", 15-17.
10. Wachman, Thermal Accommodation.
11. Lewin, Vacuum Science, 40.

## REFERENCES


1. Wachman, H.Y. The Thermal Accommodation Coefficient: A Critical Survey, J. Am. Rocket Soc., 32, (1962) 2-12.
2. Hurlburt, F.C. On the Molecular Interactions Between Gases and Solids, University of California Tech. Report # HE-150-208, (1962).
3. Patterson, G.N. Mechanics of Rarefied Gases and Plasmas, UTIAS Review #18 (1964).
4. Goodman, F.O. On the Theory of Accommodation Coefficients IV, "Simple Distribution Function Theory of Gas Solid Interaction Systems", J. Phys. Chem. Solids, 26, (1965), 85-105.
5. Logan, R.M. and Stickney, R.E. Simple Classical Model for the Scattering of Gas Atoms from a Solid Surface, J. Chem. Phys., 44, (1966), 195-201.
6. Epstein, M. A Model of the Wall Boundary Condition in Kinetic Theory, AIAA Journal, 5, (1967), 1797-1800.
7. Hinchen, J.J. and Malloy, E.S. Velocity of Molecular Beam Molecules Scattered by Platinum Surfaces, United Aircraft Research Lab, (1966).
8. Gadamer, E.O. An Optical Electron Beam Probe for Density Measurements in Rarefied Gas Flows, UTIA Report #18, (1961).
9. Muntz, E.P. Measurement of Rotational Temperature, Vibrational Temperature and Molecule Concentration in Non-Radiating Flows of Low Density Nitrogen, UTIA Report #71, (1961).

10. Marsden, D.J. Measurement of Energy Transfer in Gas-Solid Surface Interactions Using Electron Beam Excited Emission of Light, UTIA Report #101, (1964).

11. Muntz, E.P. and Marsden, D.J. Electron Excitation Applied to the Experimental Investigation of Rarefied Gas Flows, Rarefied Gas Dynamics, 2, (1962), 495-526.

12. Wachman, H.Y. The Thermal Accommodation Coefficient and Adsorption on Tungsten, Ph.D. Thesis, University of Missouri, (1957).

13. Lewin, G. Fundamentals of Vacuum Science and Technology, McGraw-Hill Book Company, (1965).

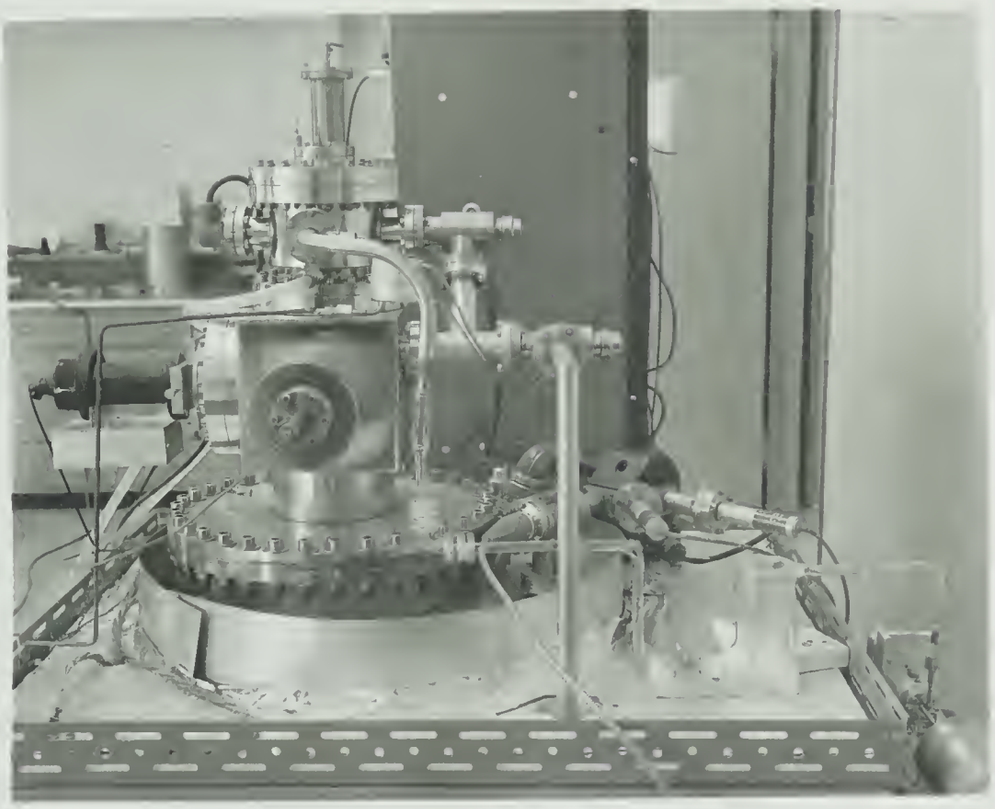

– FIGURE 1 –

– EXPERIMENTAL APPARATUS –

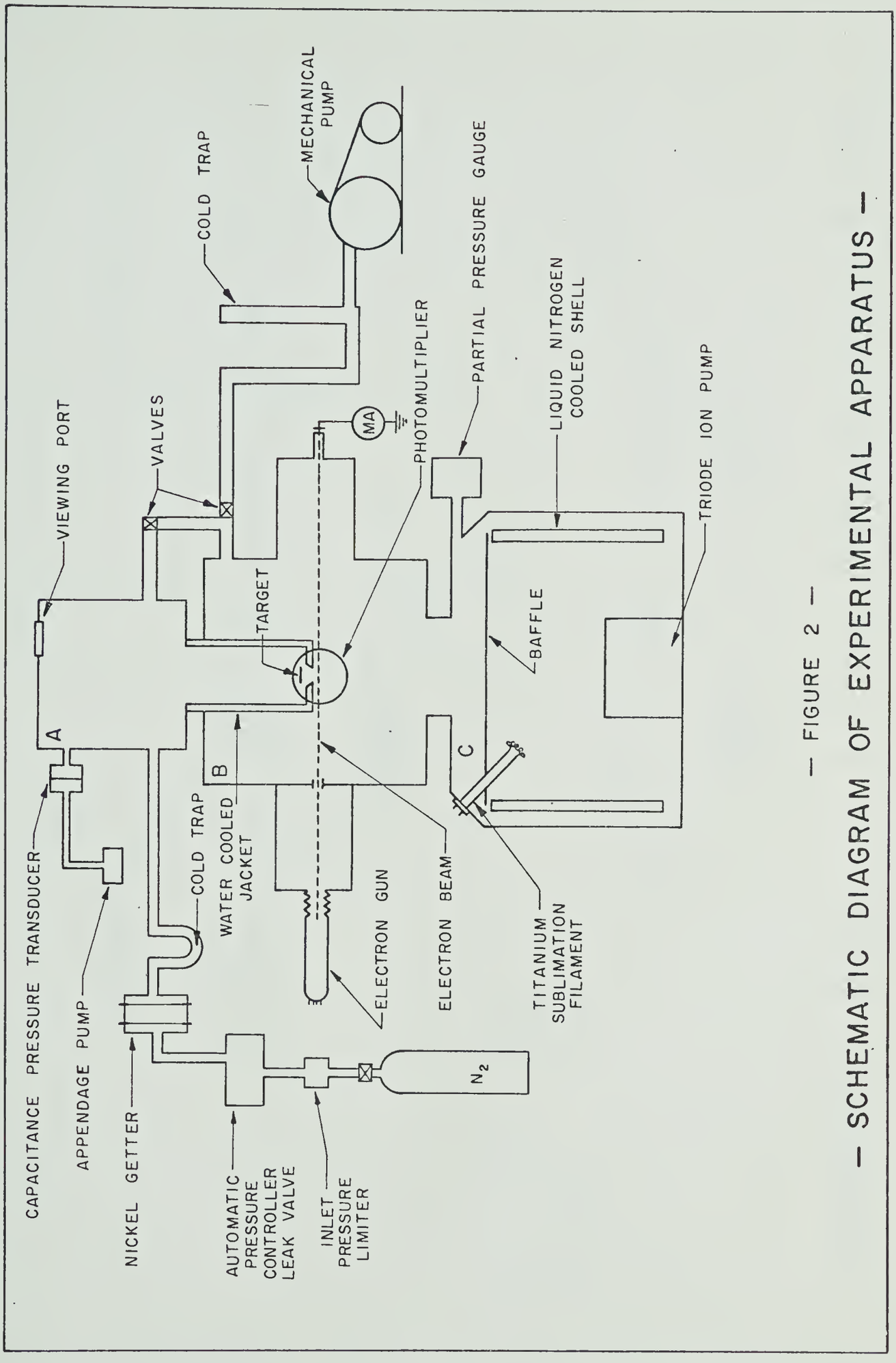


— SCHEMATIC DIAGRAM OF EXPERIMENTAL APPARATUS —

— FIGURE 2 —

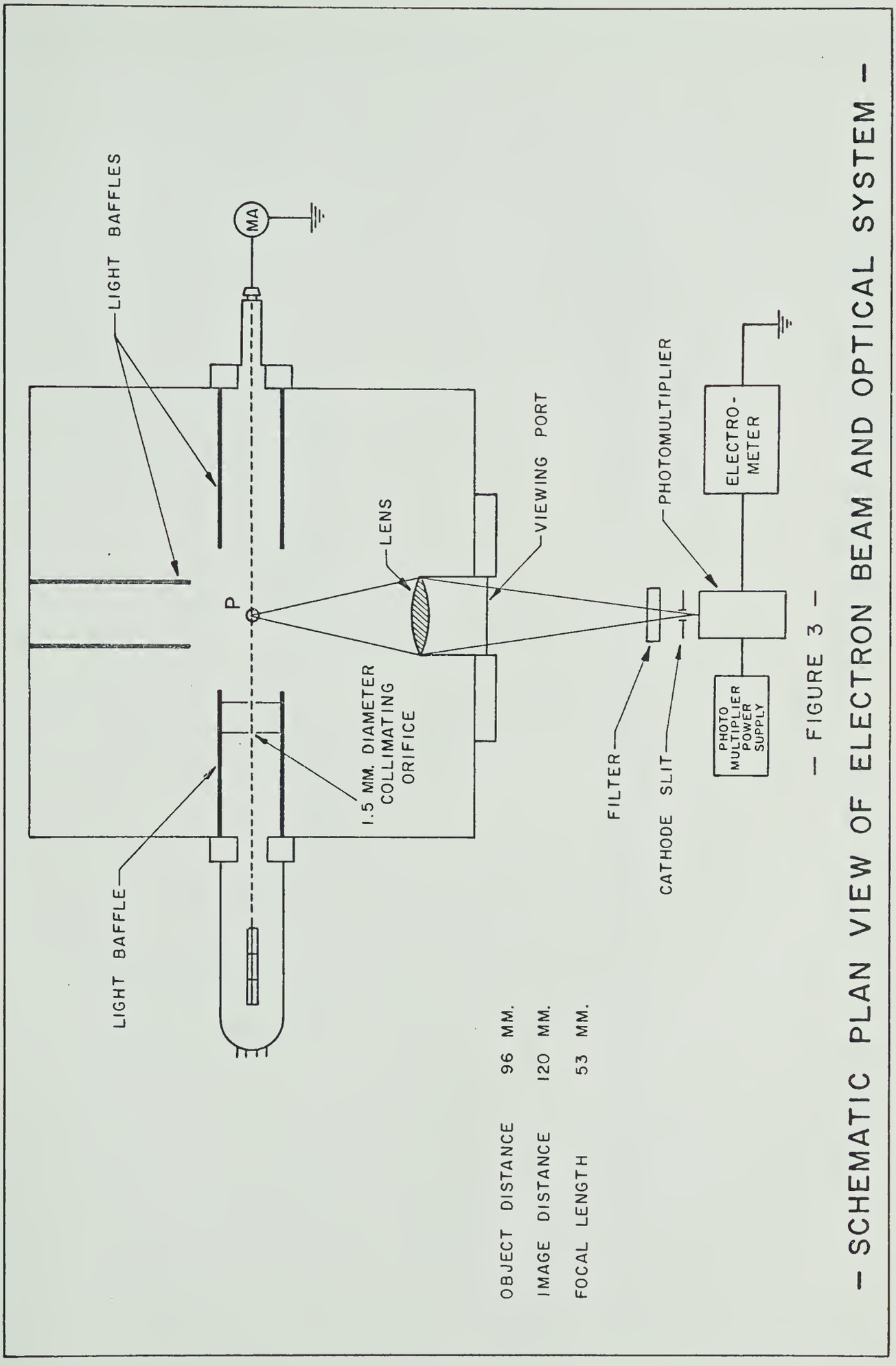


– SCHEMATIC PLAN VIEW OF ELECTRON BEAM AND OPTICAL SYSTEM –

– FIGURE 3 –

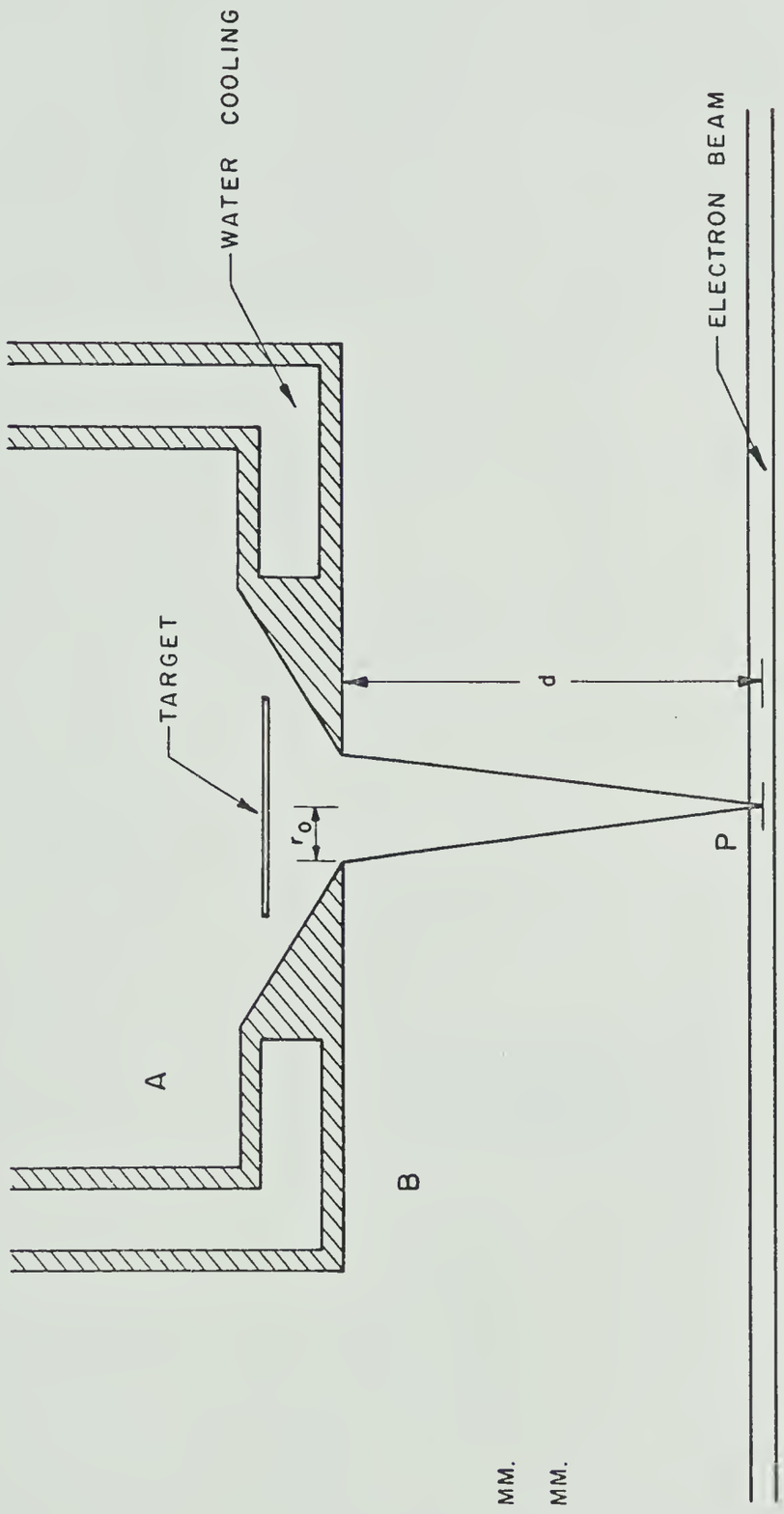


— FIGURE 4 —

— SCHEMATIC OF GEOMETRICAL ARRANGEMENT NEAR TARGET —

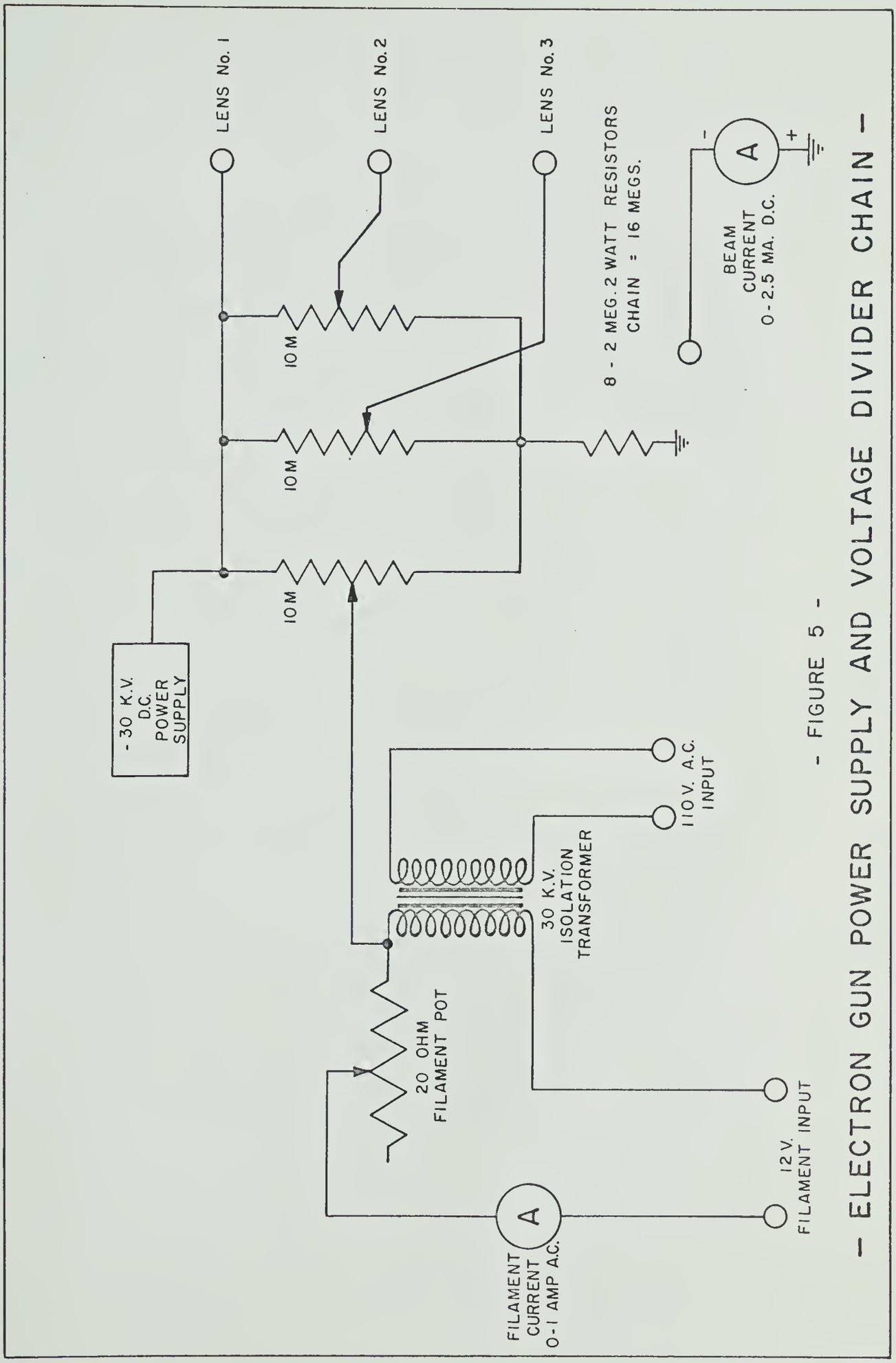


- FIGURE 5 -

- ELECTRON GUN POWER SUPPLY AND VOLTAGE DIVIDER CHAIN -

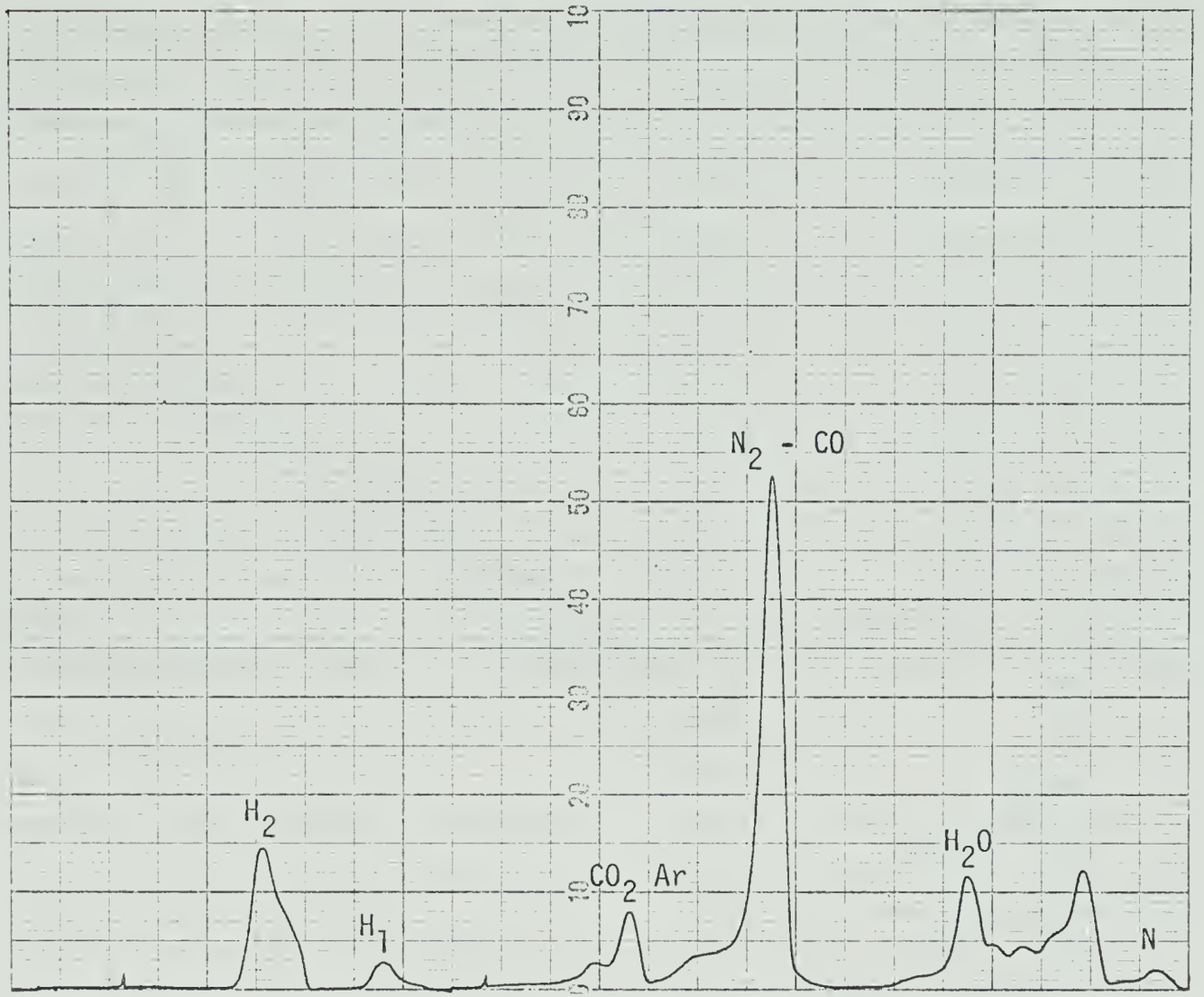


— FIGURE 6 —

— PARTIAL PRESSURE TRAVERSE —

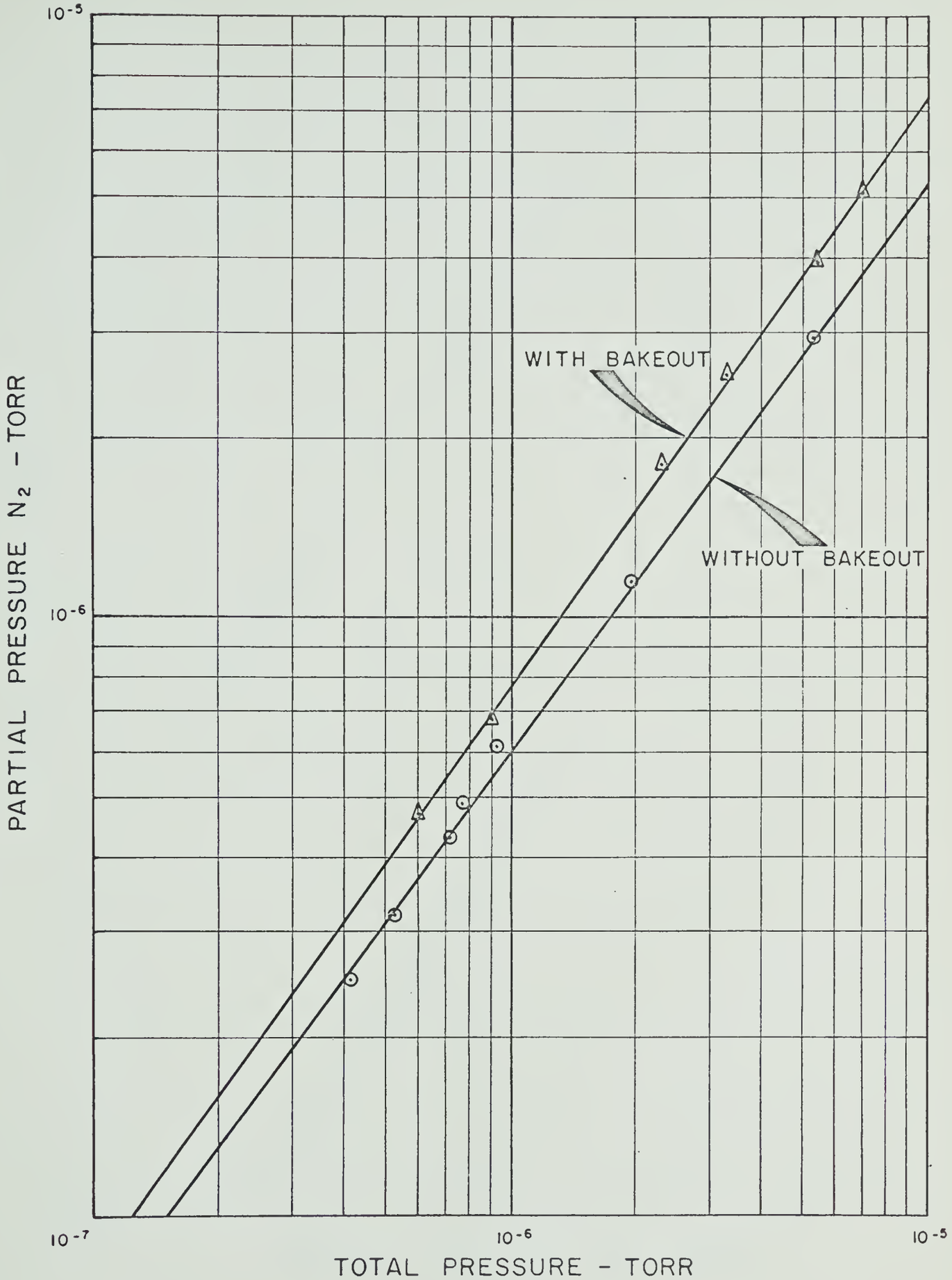


— FIGURE. 7 —

— PARTIAL PRESSURE CALIBRATION —

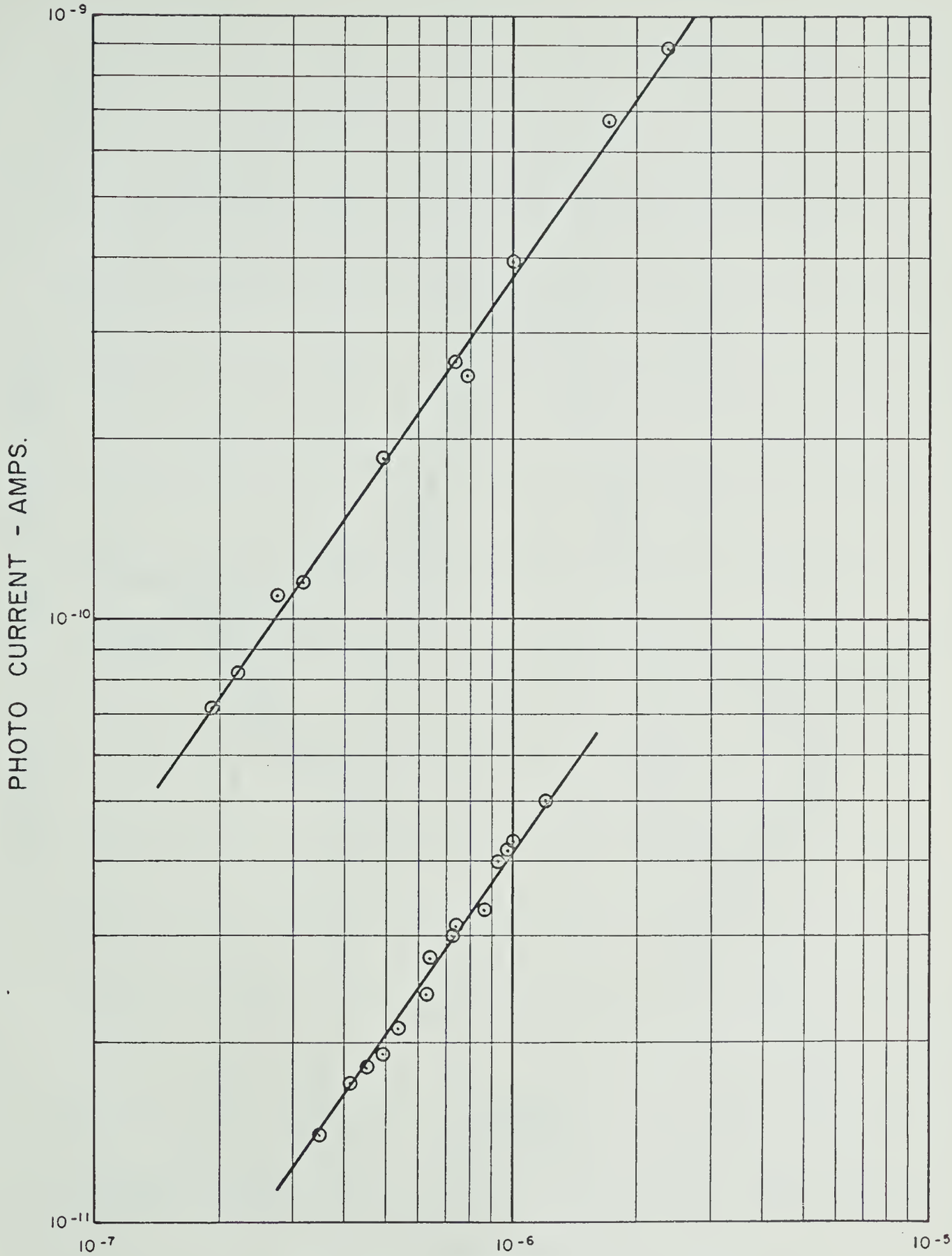


– FIGURE. 8 –

– ELECTRON BEAM CALIBRATION –

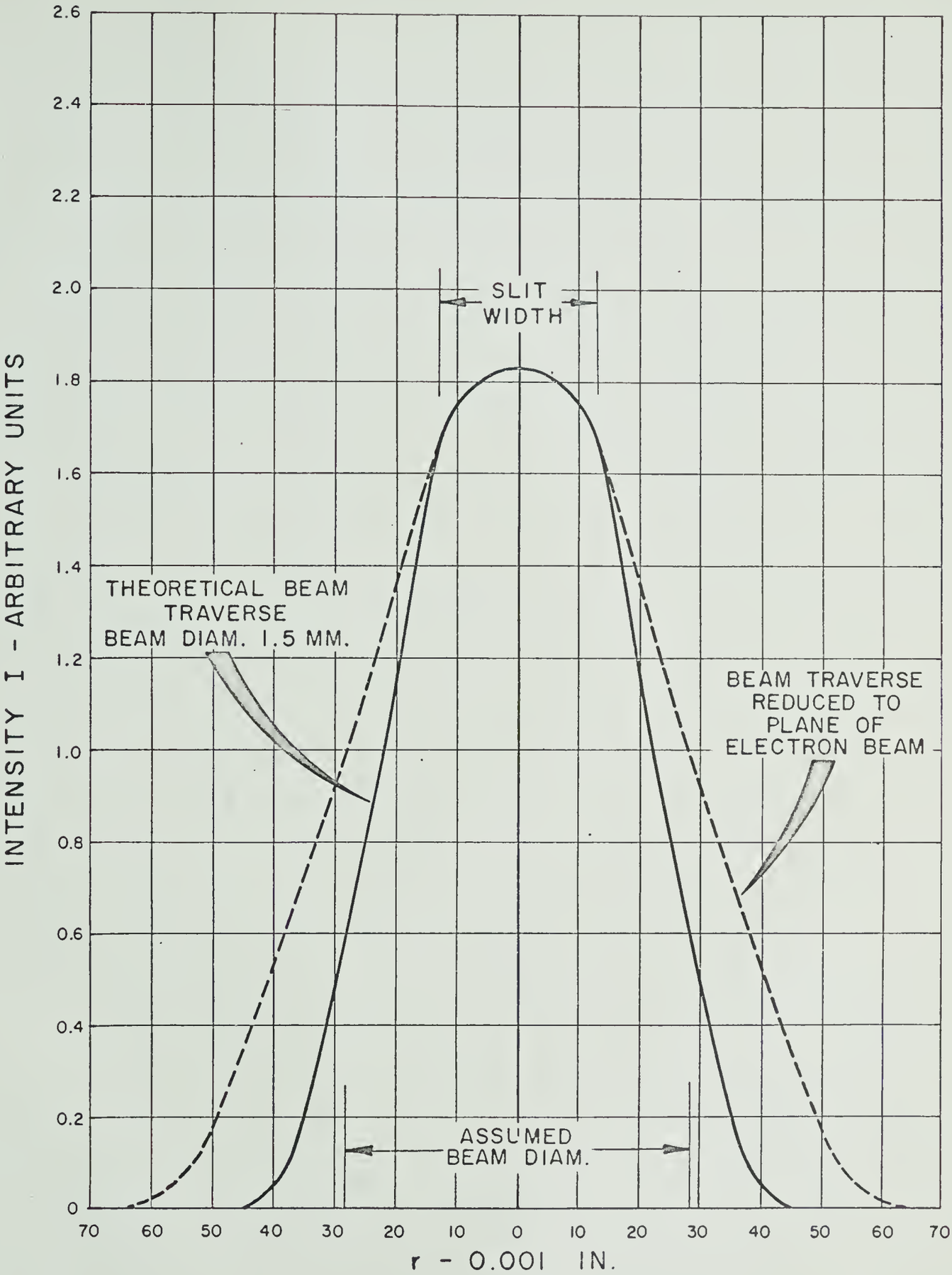


— FIGURE. 9 —

— ELECTRON BEAM TRAVERSE —